Distribution differences of macular cones measured by AOSLO: Variation in slope from fovea to periphery more pronounced than differences in total cones

Ann E. Elsner *, Toco Y.P. Chui, Lei Feng [1], Hong Xin Song, Joel A. Papay, Stephen A. Burns

Indiana University School of Optometry, 800 E. Atwater Ave, Bloomington, IN 47405, United States

ABSTRACT

Large individual differences in cone densities occur even in healthy, young adults with low refractive error. We investigated whether cone density follows a simple model that some individuals have more cones, or whether individuals differ in both number and distribution of cones. We quantified cones in the eyes of 36 healthy young adults with low refractive error using a custom adaptive optics scanning laser ophthalmoscope. The average cone density in the temporal meridian was, for the mean ± SD, $43,216 \pm 6039$, $27,466 \pm 3496$, $14,996 \pm 1563$, and $12,207 \pm 1278$ cones/mm^2 for 270, 630, 1480, and 2070 μm from the foveal center. Cone densities at 630 μm retinal eccentricity were uncorrelated to those at 2070 μm, ruling out models with a constant or proportional relation of cone density to eccentricity. Subjects with high central macula cone densities had low peripheral cone densities. The cone density ratio (2070:630 μm) was negatively correlated with cone density at 630 μm, consistent with variations in the proportion of peripheral cones migrating towards the center. We modelled the total cones within a central radius of 7 deg, using the temporal data and our published cone densities for temporal, nasal, superior, and inferior meridians. We computed an average of 221,000 cones. The coefficient of variation was 0.0767 for total cones, but higher for samples near the fovea. Individual differences occur both in total cones and other developmental factors related to cone distribution.

© 2016 Elsevier Ltd. All rights reserved.

1. Introduction

A full understanding of the mechanisms of damage and the potential to rescue cones requires normative data with sufficiently narrow confidence limits that the effects of disease or treatment can be assessed. Cone density measured *in vivo* by using adaptive optics to correct for the ocular aberrations of the human eye, along with highly magnified retinal images, has large inter-individual variations not due to methodological considerations, particularly varying with aging (Chui, Song, & Burns, 2008a; Chui et al., 2012; Liu et al., 2014; Obata & Yanagi, 2014; Song, Chui, Zhong, Elsner, & Burns, 2011). At the fovea, individual differences in young, healthy eyes are reported to have a range of 1.81:1 (Zhang et al., 2015). The decrease in cone density with aging is found across both the central and more peripheral macula, but is particularly striking in the central fovea where the cones are densely packed in young adults. Nevertheless, in the healthy older eye there is still a general decrease of cone density with increasing retinal eccentricity. The marked central decrease with aging in foveal cone density is predicted from previous imaging studies of cone photopigment density, in which the central fovea has both decreased cone photopigment and decreased macular pigment (Elsner, Burns, Beausencourt, & Weiter, 1998). Similarly, there is a decrease with increasing age in foveal phase retardation, well-modelled by the near radial symmetry in the fovea of the birefringent Henle fiber layer (VanNasdale, Elsner, Hobbs, & Burns, 2011).

Another important factor in the measurement of cone density is the axial length of the eye, particularly noted for myopic eyes even when disease is not present (Chui, Song, & Burns, 2008b; Li, Tiruveedhula, & Roorda, 2010; Obata & Yanagi, 2014; Park, Chung, Greenstein, Tsang, & Chang, 2013). The increase in axial length alone is sufficient to lead to large individual differences, and the eye shape does not necessarily change in an identical manner for all subjects (Chen et al., 1992; Clark, Elsner, & Konynenbelt, 2015). Further, the retina does not stretch in an identical manner across the retina (Chui et al., 2008b).

The numbers of specific types of cells in the retina as measured by histology, is partly determined by cell fate, which is strongly related to genetics and species differences (Jelcick et al., 2011; Whitney et al., 2011). Other developmental factors may influence retinal neural cell numbers, such as the prenatal environment including exposure to light (Rao et al., 2013).

It has long been known that foveal specialization continues long after birth in humans, requiring 4–6 yr to develop a deep foveal pit free of inner retinal cells and having densely packed cones (Provis & Hendrickson, 2008; Yuodelis & Hendrickson, 1986). Cone densities in the foveal region, as measured from human fetal tissue, were different for two eyes from the same donor at 24 weeks of age, 28,300 and 37,900 cones/mm^2. The migration of cones from the more peripheral portions of the macula leads to a fovea containing densely packed cones, and this migration is not complete until after birth. With development, cone density increases greatly in the foveal region, with estimates varying among donors but reaching 100,000–324,000 cones/mm^2 in the foveas of adults (Ahnelt, 1998; Curcio, Sloan, Kalina, & Hendrickson, 1990). The re-distribution via migration of cones can be disrupted by diabetes, even if the overall numbers of cones may not be yet decreased by disease, as compared with healthy adolescents of similar age (Tan et al., 2015).

While the total number of cones is established before birth, the distribution is not. Retinopathy of prematurity can interrupt the process of photoreceptor re-distribution, and the fovea does not assume the normal pit shape with high densities of cones (Hammer et al., 2008). We examined to what extent the large variation in cone density is also found in the total numbers of cones in the macula. Although it is technically possible to image and count all the cones within the macula (Chui et al., 2008a), this requires considerable time for both the subject and the post-processing. For many subjects, particularly older ones, the time to collect data must be limited due to the tear film stability decreasing over time during a measurement session, as well as discomfort from maintaining stable posture and steady gaze for long periods of time. In contrast, using a smaller sample of data from which the cone densities across the macula and the total cones within the central circle of 7 deg radius, i.e. 14 deg diameter, can be modelled provides the opportunity to incorporate a wider range of subjects. Further, this type of model allows using arbitrary regions of interest to provide control data for cone density, so that studies with retinal disease can be compared to normative data with narrow confidence limits of for regions of interest not tested in controls. Without a model, the pronounced decrease of cone density with eccentricity, particularly in young subjects, leads to wide confidence intervals and a lack of statistical power if too large a range of eccentricities is averaged in the normative data. Thus, we modelled the total number of cones from samples of 36 subjects in two datasets, constraining our sample to be young healthy eyes with axial lengths within a narrow range.

2. Materials and methods

2.1. General

Cone density was measured as a function of retinal eccentricity, using the Indiana Adaptive Optics Scanning Laser Ophthalmoscope (AOSLO) previously described (Burns et al., 2014; Chui et al., 2012; Song et al., 2011). Cone density data were obtained from the two groups of subjects described below: Group 1 subjects provided cone density data along the temporal, nasal, superior, and inferior meridians.

The Group 1 data were used to model the total cone count for each subject, by computing the relation between measurements of cone density along the temporal meridian to measurements of cone densities as a function of eccentricity in the temporal, nasal, superior, and inferior meridians. We modelled the relation of cone density, eccentricity, and meridian so that a total cone count could be obtained. Group 1 data were taken from our previously published data on aging (Chui et al., 2012; Song et al., 2011).

Group 2 subjects were newly recruited and data were analyzed only along the temporal meridian, where the larger retinal vessels are fewer than in the other meridians, to avoid errors in cone density due to sampling near large blood vessels (Fig. 1).

2.1.1. Participants

All subjects had a full eye examination, including a subjective refraction and fundus examination. Axial length was measured with an IOLMaster (Carl Zeiss Meditec, Dublin, CA). The length measurements were used to exclude subjects with long eyes from the study, and to correct measurements of cone density for individual differences in axial length as described previously (Chui et al., 2008a, 2008b, 2012; Song et al., 2011). These criteria avoid the alteration in cone density due to retinal disease, aging, myopia or other factors leading to an abnormal eye length and therefore inaccurate cone density.

The data from Group 1 included cone density measurements along temporal, nasal, superior, and inferior meridians, from just outside the fovea to 7 deg eccentric (Song et al., 2011). These 10 normal subjects (6 females, 4 males, 21–28 yr old, 24.4 ± 2.17) were selected from this previously analyzed younger subjects group. Some of the data were re-sampled to use the right eye or left eye to achieve the least interference of blood vessel or other artifacts and to minimize interpolation and avoid extrapolation. The eyes that contributed data had the following criteria: refractive error from −2.50 to +0.25 D (−0.60 D ± 1.13), and axial length from 23.2 to 24.7 mm (24.2 mm ± 0.497).

Group 2 included 26 additional subjects (7 females, 19 males, 18–34 yr old (24.4 ± 3.83) with healthy eyes on ophthalmic exam and who had an axial length < 26 mm. Axial length for these eyes ranged from 23.2 to 25.8 mm (24.3 ± 0.463 mm). The mean age for the total of 36 subjects was 24.4 3.42 yr. Axial length was 24.2 ± 0.61 mm.

The work was carried out in accordance with The Code of Ethics of the World Medical Association (Declaration of Helsinki). Written informed consent was obtained from all subjects, and we used consent forms and a protocol approved by the Indiana University Institutional Review Board for Human Subjects.

2.1.2. Apparatus

Cone densities were measured using a second generation AOSLO, with the methods described previously (Burns et al., 2014; Chui et al., 2012; Song et al., 2011). Retinal images covering 530 × 550 μm of the retina were acquired at 820–840 nm ± 20 nm at 185 microwatts. Sequential groups of samples, with at least 50 video frames per fixation of were collected. For all Group 1 subjects, the samples formed a "+" shape around the fovea to include temporal, nasal, superior, and inferior meridians to at least 7 deg eccentricity. For Group 2 subjects, an abbreviated protocol was used for some of the subjects to ensure the highest quality data for the temporal meridian. Data collected in overlapping samples at eccentricities from fixation up to at least 7 deg, and the shorter session avoided a decrease in contrast found for some subjects due to tear film stability decreasing over time.

### 2.2. Image processing and data analysis for cone densities

To obtain a sample of cones with all pixels having the same size on the retina, a custom dewarping program adjusted each image to counteract the image stretching due to the sinusoidal scanning of
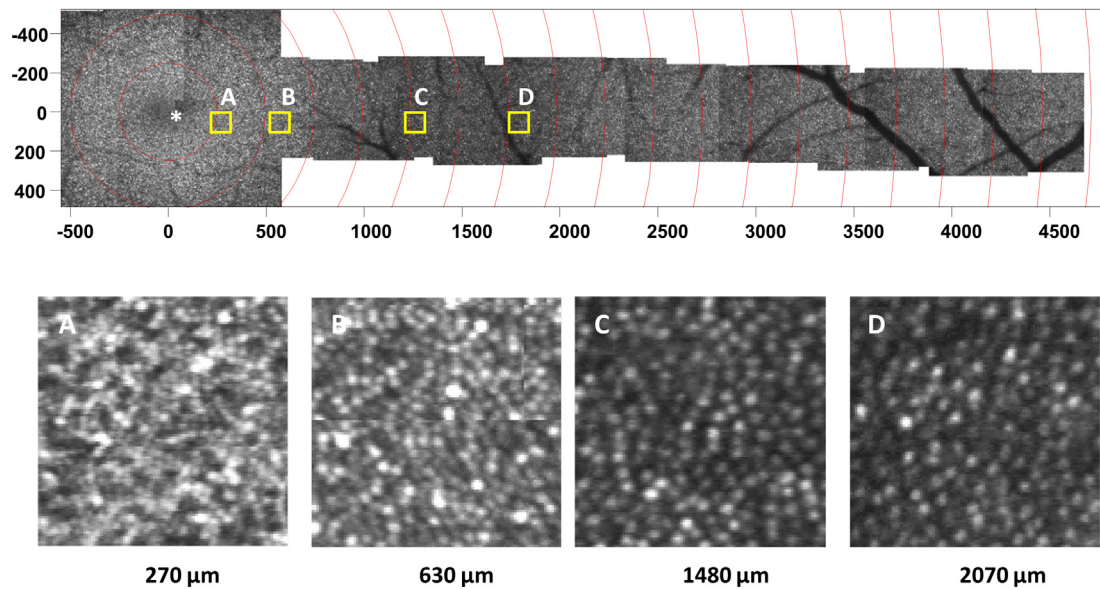
Fig. 1. Top – Cone mosaic with 4 regions of interest, plotted as a function of pixels, with the foveal center at 0. Retinal eccentricity is readily obtained after marking the location of the densest cones, and then corrected for axial length. Bottom – Samples of cones from 4 regions of interest, shown in microns, with the locations sampled corrected for axial length.

the resonant galvanometer, with all pixels in the resulting image set 1 μm with respect to the retina (Matlab, Mathworks, Natick, MA) (Chui et al., 2012; Song et al., 2011). As previously done to improve overall signal to noise ratio prior to counting the cones, two averages were obtained for each sample: 1) the average of individual frames that met alignment criteria and 2) a piecewise "Lucky Average" in which portions of the image exceeded a threshold contrast (Huang, Zhong, Zou, & Burns, 2011). The averaged data, which were in overlapping samples, were montaged to permit cone counting in selected locations with respect to the fovea.

Group 1 data were sampled in 50 μm regions of interest measured from 180 to 2160 μm, at every 90 μm, to accurately follow the steep drop in cone density near the fovea. This corresponds to approximately 0.6–7.2 deg for the emmetropic eye. Custom software was used to count each cone within a region of interest that incorporated the axial length measurement (Matlab, Mathworks, Natick, MA) (Chui et al., 2012; Song et al., 2011). For Group 2, cones were measured at a nominal 270, 630, 1480, and 2070 μm, or 0.9 to 6.9 deg, from the foveal center for the temporal meridian only, to minimize potential artifact in counting the cones due to shadowing from large retinal vessels. The region of interest was increased to 100 μm with respect to the retina and a "+" shape with extra pixels above, below, to the right, and to the left of the region of interest facilitated counting cones at the edge (Fig. 2). The decrease in cone density with retinal eccentricity is less steep at 270 μm compared with 180 μm (Song et al., 2011). Therefore, using the larger region of interest for Group 2 data led to less artifact than it would have for Group 1, and less artifact for cone counts at 630 μm than 270 μm. Additional details concerning the procedure and test-retest reliability of this cone counting method are previously published (Song et al., 2011; Chui et al., 2012). These studies find differences in cone density of only 2% between two graders for normal eyes, and no change over 6 months other than specific cones appearing brighter or dimmer. The Group 2 data had less densely analyzed data and did not include data as close to the foveal center as Group 1 data: 270, 630, 1480, and 2070 μm from the foveal center. To avoid underestimating cone density in the region of interest nearest the fovea, quantitative comparisons across eccentricities were made outside the central fovea, at eccentricities of 630 μm and 2070 μm. (See Table 1 for Coefficient of
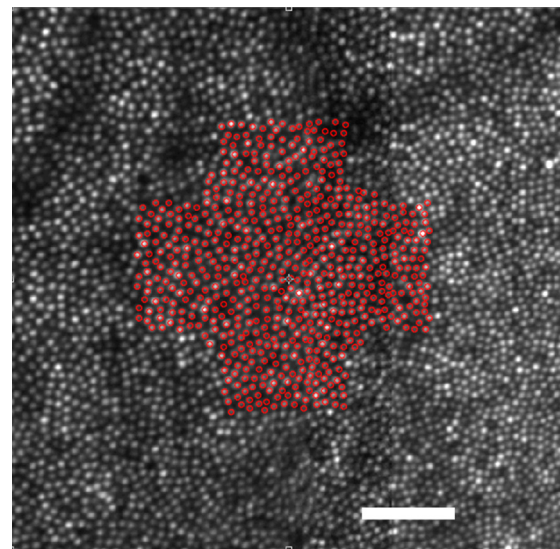
Fig. 2. Cone mosaic with cones marked in red for a sample at 630 μm from the fovea, after correction for axial length. This method was used for all of Group 2 subjects, so that cones on the left, right, top, and bottom edges of the 100 × 100 μm region of interest were correctly included. The scale bar represents 60 μm or approximately 0.2 deg on the retina.

Variation.) All quantitative comparisons are based on the data from the temporal meridian, with the exception that the value for total cones for each subject is scaled with the average from all for meridians.

3. Results for cone densities

Cone density decreased with eccentricity, with considerable variation among the 36 subjects at each eccentricity (Table 1). Cone densities varied across subjects at all 4 eccentricities, with a roughly 1.75:1 variation from maximum to minimum at the region of interest nearest to the fovea. The variability was greatest in the centralmost measurements whether the metric was the

Table 1
Cone densities measured with adaptive optics scanning laser ophthalmoscopy in 36 subjects.

Microns from fovea	270	630	1480	2070
Mean cone density (cones/mm^2)	43216	27466	14996	12207
Standard Deviation (cones/mm^2)	6039	3496	1563	1278
Coefficient of Variation	0.140	0.127	0.104	0.105

standard deviation or the coefficient of variation, i.e. for both absolute and relative metrics of variability. There is a broad distribution of cone densities at each eccentricity, and there were no clusters of cone densities apparent at any eccentricity. Samples of particular interest are: A) 630 µm for the mean + SD (27,466 ± 3496 cones/mm^2), which is in a cone rich area but not in the central fovea where large aging changes occur and B) 2070 µm (12,207 ± 1278 cones/mm^2), which is approximately 7 deg eccentric and where rods begin to outnumber cones.

Subjects with higher cone densities near the fovea, such as at 630 µm, can have visibly fewer cones more peripheral to the fovea, at 2070 µm (Fig. 3). The decrease of cone density with eccentricity is so large in the sample of young, emmetropic subjects that it is difficult to observe the relation between cone density and retinal eccentricity for an individual subject (Fig. 4). When including both Groups 1 and 2, the cone density at 630 µm was uncorrelated with that at 2070 µm (r = 0.120, p = 0.486) (Fig. 5). We provided a simple linear equation and evaluated the parameters:

$$\text{cone density (2070 microns)} = a + b * \text{cone density (630 microns)}. \quad (1)$$

For our 36 subjects, a = 11,000 cones/mm^2 and b = 0.44, but the relation is so weak as to not provide support for such a simple linear model. This lack of correlation indicates that individuals with high cone density at one location do not necessarily have cone densities relatively higher than the population at other locations. This finding precludes the possibility of modelling cone densities at unmeasured locations by merely using a different scalar factor, i.e. a larger or smaller value of the parameter a, to increase or
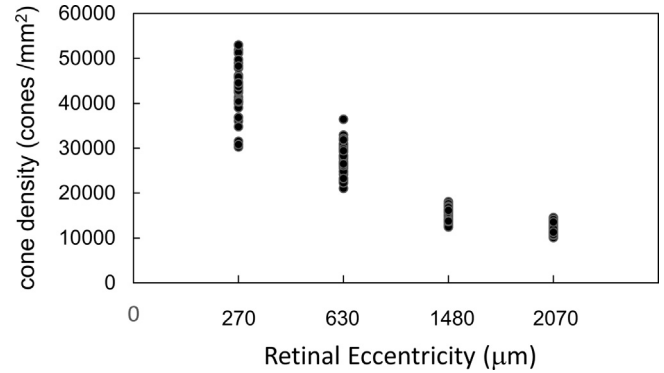
Fig. 4. Cone densities as a function of retinal eccentricity for 36 young, healthy subjects with normal eye length. Inter-individual variability increases nearer the fovea.
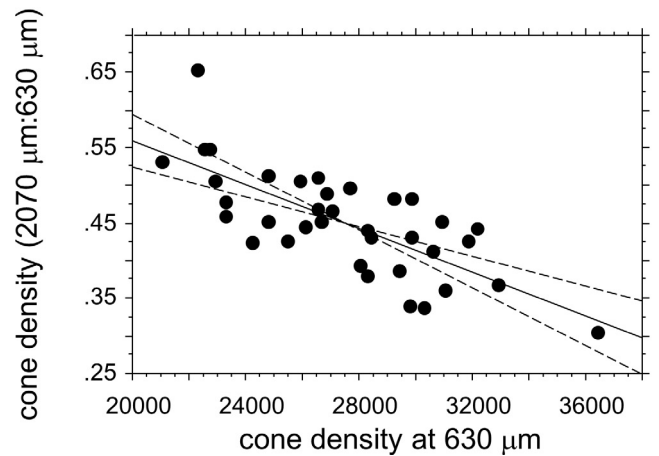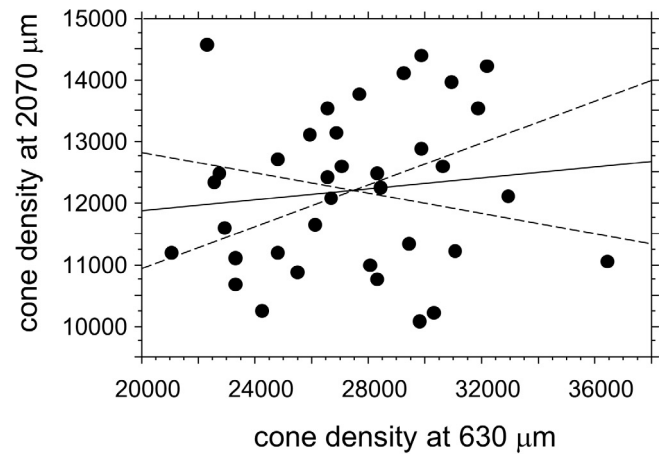
Fig. 5. Top – Cone densities at 2070 µm retinal eccentricity for 36 subjects plotted as a function of their cone densities at 630 µm, showing the lack of correlation. The linear fit was cone density at 2070 µm = 11,000 + 0.44 * cone density at 630 µm. R^2 = 0.014. Bottom – The ratio of cone density at 2070 µm to cone density at 630 µm for each subject, abbreviated as cone densities (2070 µm:630 µm), for 36 subjects plotted as a function of their cone densities at 630 µm. There is a strong negative correlation. The solid line provides the linear fit, and dashed lines are the 95% confidence limits on slope. The linear fit was cone density (2070 µm:630 µm) = 0.85 − 1.45 E^{-5} * cone density at 630 µm. R^2 = 0.544.
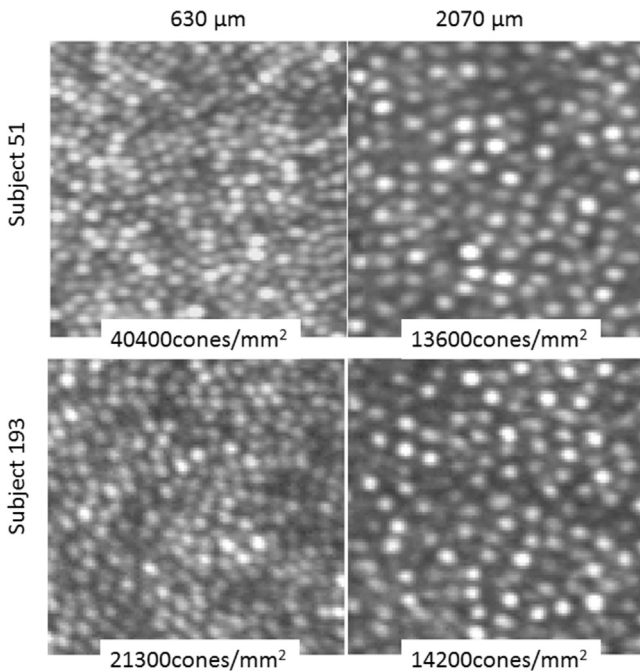
Fig. 3. Cone mosaics and cone densities at 630 and 2070 µm eccentricities for two subjects, showing that the top subject with a higher cone density at 630 µm but a lower cone density at 2070 µm.

decrease an individual's cone densities with respect to a template. Similarly another model that is ruled out is one in which there is a proportional increase/decrease related to eccentricity that multiplies the cone density at one location to obtain the expected number of cones at another. That is, varying the proportional increase is achieved by using a larger or smaller value for the slope parameter b, but still requires that there is a significant correlation.

An alternative model was tested, in which the migration of more peripheral cones towards the fovea influences the distribution of cones across the macula, where

cone density (2070 microns : 630 microns)

$$= a + b * \text{cone density (630 microns)}. \qquad (2)$$

Therefore, instead of the cone densities being correlated at different locations across the central macula, cone density 2070:cone density 630 μm is strongly correlated, but negatively, to cone density at 630 μm (r = −0.738, p = 0.0001). For this model, a = 0.85 and b = −0.0000145. Thus, cones in the periphery are relatively fewer for those subjects with high cone density nearer the fovea. This model supports the idea that cone density is strongly influenced by foveal specialization when cones redistribute by migrating from more peripheral to more central locations during development. This model and these parameters fit well the data of young healthy eyes that have axial lengths that are typical for low refractive errors.

4. Modelling cone density and total cones within the central radius of 7 deg (central 14 deg diameter)

### 4.1. Model of cone density as a function of retinal eccentricity

To allow the computation of cone density at desired locations within the central 14 deg or approximately 4200 μm, as well as the total cones within the central 14 deg, we modelled the data of Group 1 and Group 2. First, the results above, which showed no correlation of cone density at 630 μm to that at 2070 μm, indicated that neither a constant scalar factor nor a proportion that scaled with eccentricity provided a good fit across the central 14 deg of retina. To provide an alternative model of the cone density data, we first examined whether there was a simple, analytical function that would characterize the cone density data across retinal eccentricity An exponential model has been shown previously with our data, but with a fewer number of subjects (Song et al., 2011). We investigated whether the exponential fit would fit our dataset of 36 subjects well enough to be able to interpolate between points.

We performed a natural log transform on the data, then fit each subject's data with a linear model. Specifically, using the same 4 regions of interest, 270, 630, 1480, and 2070 μm, we fit the following model.

ln (cone density at x eccentricity in microns)

$$= a + b * \text{eccentricity in microns}. \qquad (3)$$

For our sample, a = 10.7 ± 0.146, and b = −0.0692 ± 0.00980. This single exponential model provided an excellent fit with low errors for all except one subject, R^2 = 0.937 ± 0.387. The R^2 values were >0.90 for all subjects except one, who had R^2 = 0.757. This subject had a relatively high cone density at 270 μm, and then a steep fall-off to cone density at 630 μm.

For most subjects, a slightly steeper function than that generated by the exponential model used would have provided an even better model, i.e. a slightly steeper slope from 270 to 630 μm, or either/both of the 630 or 1480 μm data falling slightly lower than expected from 270 or 2070 μm data (Fig. 6). However, the potential improvement in the fits is small given the excellent fits. It could be
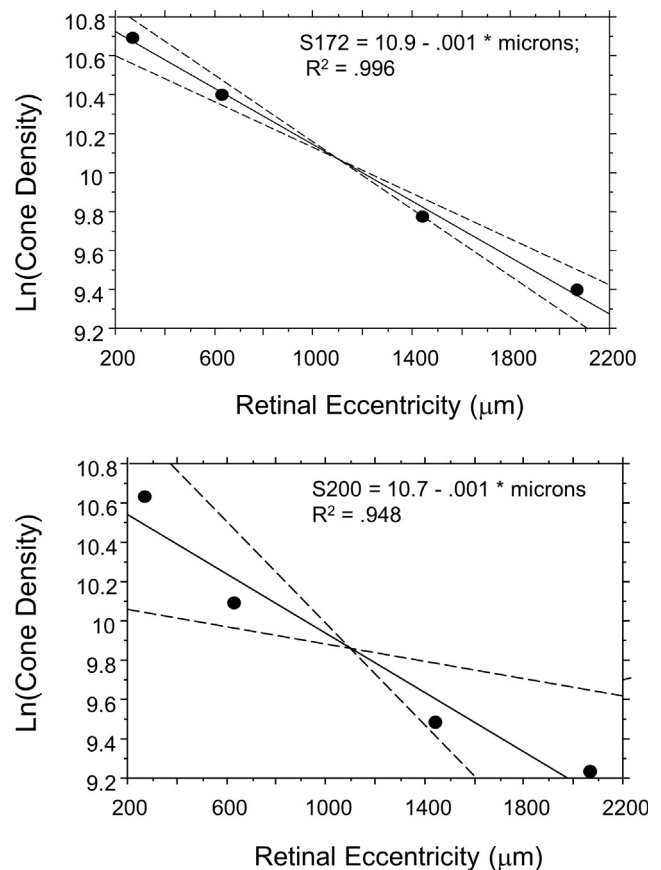
Fig. 6. Top – Natural logarithm of cone density at 270, 630, 1480, and 2070 μm eccentricity for a subject with an excellent fit to a single exponential model. Bottom – Natural logarithm of cone density at 270, 630, 1480, and 2070 μm eccentricity for a subject with typical fit to a single exponential model, with a high proportion of variance accounted for. There is still a small and systematic deviation: for many subjects one or both of the data points between 270 and 2070 μm fall slightly below the fit line. The solid line provides the linear fit, and dashed lines are the 95% confidence limits on slope.

the case that a systematic improvement across the 36 subjects would require another parameter, or merely a slight change in the value of the base logarithm that may move the curve closer to some of the data points in some cases. The resulting error in using the exponential function is that there will be a slight under-estimation for cone density at the fovea relative to about 3 deg or 900 μm. The fovea has a high cone density but little retinal area, so contributes very few cones overall to the central 14 deg, i.e. a radius of 7 deg or 2100 μm. The centralmost foveal cones, which have the highest cone densities in young, healthy subjects, number only 300–500 cones (Ahnelt, 1998).

4.2. Model of total cones from temporal cone data

For Group 1, we computed the ratio of the density of temporal cones to the average of all 4 meridians, using all 12 potential subjects, despite some having missing data, with finely sampled data at 4 meridians to increase statistical power (Song et al., 2011). The temporal and nasal meridians have higher cone densities than inferior and superior meridians, and we analyzed our data to show the similar relation among these meridians over a wide range of eccentricities, with the exception being near the optic nerve head. The ratio of the average to the temporal cone density was approximately constant across retinal eccentricity (0.926 ± 0.0247). The linear regression indicated no trend with eccentricity, and instead
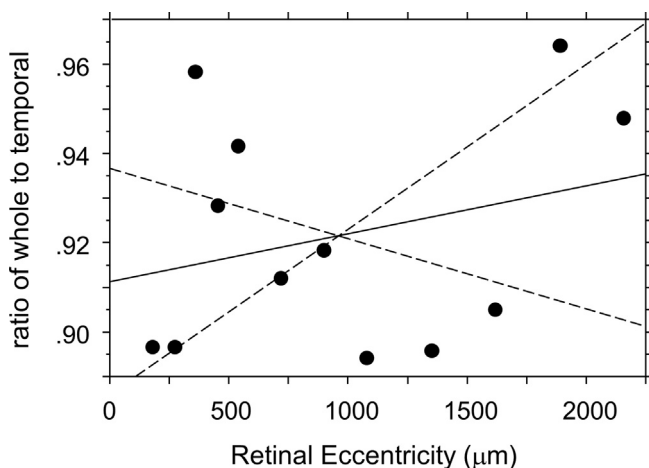
the highest and lowest ratios occurring across a variety of eccentricities (Fig. 7). The ratio varied over a small range (0.894–0.964), the slope had no clear trend, and the slope could not be distinguished from 0, with $R^2 = 0.076$, p = 0.386. For the superior and inferior meridians, the ratio was 1.20 and 1.17. The superior meridian ratio was uncorrelated with eccentricity, $R^2 = 0.189$.

The inferior meridian ratio was correlated with eccentricity, i.e. $R^2 = 0.363$, but in fact the ratios across eccentricities had a slope of nearly 0, i.e. −0.0000944. The nasal eccentricities, like the temporal eccentricities, had a higher ratio when compared with the average cone densities, 1.02. This meridian had the highest correlation, $R^2 = 0.829$, and a positive slope 0.000121, indicating higher cone densities nearer the optic nerve head and the potential for higher variability of the model at those locations. Due to the stability of the fits across eccentricity and the minimization of errors because of few large retina blood vessels, the average ratio of temporal cones was used to scale each subject's data in the pooled set of 36 subjects to compute the overall numbers of cones in the macula.
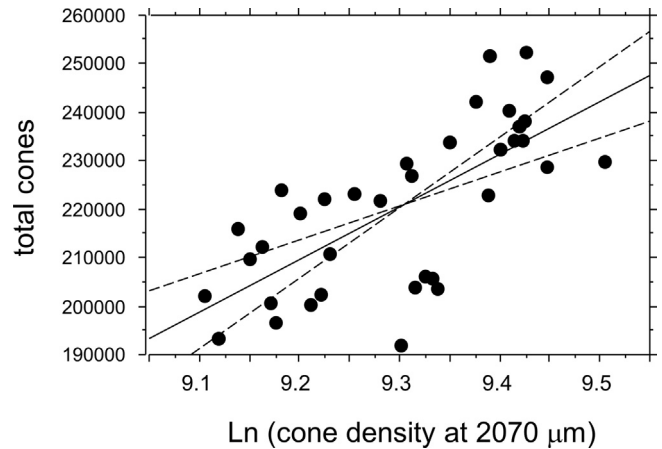
We divided the retina into 29 narrow, concentric areas, and computed the area covered on the retina and cone density, assuming a flat area that contained the number of cones found at the outer edge. The number of cones was obtained by interpolating, using the exponential model. We did not extrapolate to more peripheral data, since our computation did not include these areas and small errors would magnify when multiplied by the large retinal areas. For each of these areas and for each subject, we computed the mean cone density and the coefficient of variation for each area, pooled across all 36 subjects.

The total number of cones in a circular area of the macula with a radius of 7 deg averaged 221,000 ± 16,900 for the 36 subjects (Fig. 8). The coefficient of variation for the overall total was 0.0767. The computed coefficient of variation for the areas nearer the fovea were typically larger, and the coefficient of variation from the data was significantly larger for cone densities at 270 μm compared with total cones, (p < 0.001). Table 1 shows that largest coefficient of variation for the 4 sampled regions of interest was the data point nearest the fovea, i.e. 0.14. The three regions of interest farther away also had cone densities significantly less variable across subjects (p < 0.001).

The total number of cones was significantly correlated with the numbers of cones at 2070 μm, p < 0.00001. These findings indicate that the high variability among individuals does not depend solely

Fig. 8. Total cones computed from the model plotted as a function of cone density at 2070 μm retinal eccentricity for 36 subjects, showing a strong positive correlation. The solid line provides the linear fit, and dashed lines are the 95% confidence limits on slope. The linear fit of total cones = −784179 + 108022 * ln cone density at 2070 μm. $R^2 = 0.499$.

on total cone numbers, and that the proportion of cones that migrated to the fovea is also an important cause of individual differences in cone distribution.

5. Discussion

The large variability in cone density at a given location on the retina is known to depend upon meridian, age, eye length/refractive error, and health of the retina measured in numerous laboratories with *in vivo* methods (Chui et al., 2008a, 2012; Liu et al., 2014; Li et al., 2010; Obata & Yanagi, 2014; Park et al., 2013; Song et al., 2011; Tan et al., 2015) as well as with *ex vivo* methods (Ahnelt, 1998; Curcio et al., 1990). However, our results indicate that the variability of total cones across a large portion of the macula is much less among individuals, when the eye is healthy, eye length is normal, and age is restricted to young adult ages.

We reject the model of cone distribution that accounts for the variability among subjects to be merely a change in total cone numbers across individuals, since there is no correlation between cone density at 630 μm and 2070 μm from the fovea. This lack of correlation indicates that there is not a nomogram for cone density vs. eccentricity that scales across individuals according to total cones. We also reject a similar model of cone distribution that requires individuals with a high density of cones near the fovea of cones also have the highest cone densities at greater eccentricities, such as a model in which individuals differ in overall cone numbers with a proportional decrease with increasing eccentricity. Instead, many individuals with the highest cone densities near the fovea have the lowest cone densities in the periphery. There is a strong but negative correlation between the ratio of cone density at 2070 μm to 630 μm from the fovea vs 630 μm. These findings are consistent with total cones being more similar across individuals, but cones in the periphery migrating to the fovea in differing proportions.

For the two types of data that we used to model cone density and total cones, there were advantages and disadvantages to the methods used. For the Group 1 data (Song et al., 2011), using a small region of interest allowed much more closely spaced samples, and provided better independence of sampling near the fovea where there is a steep decrease in cone density with increasing retinal eccentricity. However, the smaller region of interest allows fewer cones to be counted. The smaller area provides less tolerance when there is a focal artifact present. For the Group 2 data, mea-

Fig. 7. Ratio of cone densities averaged across the horizontal, vertical, nasal, and temporal meridians to the temporal meridian only, abbreviated as ratio of whole to temporal. For 12 young and healthy subjects the variation does not depend upon retinal eccentricity. The solid line provides the linear fit, and dashed lines are the 95% confidence limits on slope. The linear fit of the ratio of whole to temporal = 0.911 + 1.07 E^{-5} * eccentricity in μm. $R^2 = 0.076$.

suring only the temporal meridian helped us space the samples accurately because there were relatively few large blood vessels to avoid. Using the temporal meridian only led to requiring us to estimate the cone density over the rest of the retina. However, we had all 4 meridians on 12 subjects. The ratio of cone density for the temporal retina to the other 4 meridians was well described by a constant across both subjects and meridian.

Future work requires that we determine whether the computations used for young, healthy, nearly emmetropic eyes are correct for a wider sample of subjects. The lack of correlation across retinal eccentricity in the young, healthy, nearly emmetropic eyes may hold, such as in the case of retinal disease that kills photoreceptors. We have not ascertained whether the ratio of temporal cone density to the total cone density is constant across eccentricities for older subjects or in myopic or hyperopic eyes. It is not known whether in the presence of focal retinal disease the cones move along a meridian towards or away from the fovea, or redistribute in other directions, and over what distances and time period. Given the geographic atrophy that occurs in age-related macular degeneration, when a wave of alterations to the retinal pigment epithelium and retina leads to striking and focal decreases in cones (Sarks, Sarks, & Killingsworth, 1988), then the relation of cone density to eccentricity clearly must differ in some individuals from that shown here.

Disclosure

Ann E. Elsner None, Toco Y.P. Chui none, Lei Feng none, Hongxin Song none, Joel A. Papay none, and Stephen A. Burns none.

Acknowledgements

References

Ahnelt, P. K. (1998). The photoreceptor mosaic. Eye, 12, 531–540.
Burns, S. A., Elsner, A. E., Chui, T. Y., Vannasdale, D. A., Jr, Clark, C. A., Gast, T. J., ... Phan, A. D. (2014). In vivo adaptive optics microvascular imaging in diabetic patients without clinically severe diabetic retinopathy. Biomedical Optics Express, 5, 961–974. http://dx.doi.org/10.1364/BOE.5.000961. eCollection 2014.
Chen, J. F., Elsner, A. E., Burns, S. A., Hansen, R. M., Lou, P. L., Kwong, K. K., & Fulton, A. B. (1992). The effect of eye shape on retinal responses. Clinical Vision Science, 7. 521Y30.
Chui, T. Y., Song, H., & Burns, S. A. (2008a). Adaptive-optics imaging of human cone photoreceptor distribution. Journal of the Optical Society of America. A, Optics, Image Science, and Vision, 25, 3021–3029.
Chui, T. Y., Song, H., & Burns, S. A. (2008b). Individual variations in human cone photoreceptor packing density: Variations with refractive error. Investigative Ophthalmology & Visual Science, 49, 4679–4687.
Chui, T. Y., Song, H., Clark, C. A., Papay, J. A., Burns, S. A., & Elsner, A. E. (2012). Cone photoreceptor packing density and the outer nuclear layer thickness in healthy subjects. Investigative Ophthalmology & Visual Science, 53, 3545–3553.
Clark, C. A., Elsner, A. E., & Konynenbelt, B. J. (2015). Eye shape using partial coherence interferometry, autorefraction, and SD-OCT. Optometry and Vision Science, 92, 115–122.
Curcio, C. A., Sloan, K. R., Kalina, R. E., & Hendrickson, A. E. (1990). Human photoreceptor topography. Journal of Comparative Neurology, 292, 497–523.
Elsner, A. E., Burns, S. A., Beausencourt, E., & Weiter, J. J. (1998). Foveal cone photopigment distribution: small alterations associated with macular pigment distribution. Investigative Ophthalmology & Visual Science, 39, 2394–2404.
Hammer, D. X., Iftimia, N. V., Ferguson, R. D., Bigelow, C. E., Ustun, T. E., Barnaby, A. M., & Fulton, A. B. (2008). Foveal fine structure in retinopathy of prematurity: An adaptive optics Fourier domain optical coherence tomography study. Investigative Ophthalmology & Visual Science, 49, 2061–2070.
Huang, G., Zhong, Z., Zou, W., & Burns, S. A. (2011). Lucky averaging: Quality improvement on adaptive optics scanning laser ophthalmoscope images. Optics Letters, 36, 3786–3789.
Jelcick, A. S., Yuan, Y., Leehy, B. D., Cox, L. C., Silveira, A. C., Qiu, F., et al. (2011). Genetic variations strongly influence phenotypic outcome in the mouse retina. PLoS ONE, 6, e21858.
Li, K. Y., Tiruveedhula, P., & Roorda, A. (2010). Intersubject variability of foveal cone photoreceptor density in relation to eye length. Investigative Ophthalmology & Visual Science, 51, 6858–6867.
Liu, B. S., Tarima, S., Visotcky, A., Pechauer Cooper, A. R. F., Landsem, L., et al. (2014). The reliability of parafoveal cone density measurements. British Journal of Ophthalmology, 98, 1126–1131.
Obata, R., & Yanagi, Y. (2014). Quantitative analysis of cone photoreceptor distribution and its relationship with axial length, age, and early age-related macular degeneration. PLoS ONE, 14(9), e91873. http://dx.doi.org/10.1371/journal.pone.0091873.
Park, S. P., Chung, J. K., Greenstein, V., Tsang, S. H., & Chang, S. (2013). A study of factors affecting the human cone photoreceptor density measured by adaptive optics scanning laser ophthalmoscope. Experimental Eye Research, 108, 1–9.
Provis, J. M., & Hendrickson, A. E. (2008). The foveal avascular region of developing human retina. Archives of Ophthalmology, 126, 507–511.
Rao, S., Chun, C., Fan, J., Kofron, J. M., Yang, M. B., Hegde, R. S., & Lang, R. A. (2013). A direct and melanopsin-dependent fetal light response regulates mouse eye development. Nature, 494(7436), 243–246. PMID: 23334418.
Sarks, J. P., Sarks, S. H., & Killingsworth, M. C. (1988). Evolution of geographic atrophy of the retinal pigment epithelium. Eye (London, England), 2, 552–577.
Song, H., Chui, T. Y., Zhong, Z., Elsner, A. E., & Burns, S. (2011). Variation of cone photoreceptor packing density with retinal eccentricity and age. Investigative Ophthalmology & Visual Science, 52, 7376–7384.
Tan, W., Wright, T., Rajendran, D., Garcia-Sanchez, Y., Finkelberg, L., Kisilak, M., et al. (2015). Cone-photoreceptor density in adolescents with type 1 diabetes. Investigative Ophthalmology & Visual Science, 56, 6339–6343. http://dx.doi.org/10.1167/iovs.15-16817.
VanNasdale, D. A., Elsner, A. E., Hobbs, T., & Burns, S. A. (2011). Foveal phase retardation changes associated with normal aging. Vision Research, 51, 2263–2272.
Whitney, I. E., Raven, M. A., Ciobanu, D. C., Poché, R. A., Ding, Q., Elshatory, Y., et al. (2011). Genetic modulation of horizontal cell number in the mouse retina. Proceedings of the National Academy of Sciences of the United States of America, 108, 9697–9702. PMID: 21576457.
Yuodelis, C., & Hendrickson, A. (1986). A qualitative and quantitative analysis of the human fovea during development. Vision Research, 26, 847–855.
Zhang, T., Godara, P., Blanco, E. R., Griffin, R. L., Wang, X., Curcio, C. A., et al. (2015). Variability in human cone topography assessed by adaptive optics scanning laser ophthalmoscopy. American Journal of Ophthalmology, 160, 290–300.